Composition and Dynamics of the Nucleolinus, a Link Between the Nucleolus and Cell Division Apparatus in Surf Clam (*Spisula*) Oocytes

Mark C. Alliegro,[1] Steven Hartson,[2] and Mary Anne Alliegro[1]

[1]From the Josephine Bay Paul Center for Comparative Molecular Biology & Evolution, The Marine Biological Laboratory, Woods Hole, MA 02543

[2] Department of Biochemistry & Molecular Biology, Oklahoma State University, Stillwater, OK 74078

*Running title: *Link between the nucleolus and cell division apparatus*

To whom correspondence should be addressed: Mark C. Alliegro, Josephine Bay Paul Center, Marine Biological Laboratory, 7 MBL Street, Woods Hole, MA 02543, USA, Tel,: 508-289-7419; E-mail: malliegro@mbl.edu

Key Words: Centrosome, spindle, centrosomal RNA, nucleolinus, centriole, cell cycle

Background: The nucleolinus is a little known cellular structure associated with the nucleolus that was discovered over 150 years ago.
Results: It contains a unique set of molecules associated with cell division.
Conclusion: Combined with laser microsurgery experiments, the observations suggest a role for the nucleolinus in spindle formation.
Significance: The nucleolinus appears to be a tangible link between the nucleolus and cell division apparatus.

SUMMARY

The nucleolinus is a little-known cellular structure, discovered over 150 years ago (1) and thought by some investigators in the late 19th to mid-20th century to function in the formation of the centrosomes or spindle. A role for the nucleolinus in formation of the cell division apparatus has recently been confirmed in oocytes of the surf clam, *Spisula solidissima* (2). However, we know so little about the composition and dynamics of this compartment, it is difficult to construct mechanistic hypotheses or even to be sure that prior reports were describing analogous structures in the cells of mammals, amphibians, plants, and other organisms where it was observed. Surf clam oocytes are an attractive model to approach this problem because the nucleolinus is easily visible by light microscopy, making it accessible by laser microsurgery as well as isolation by common cell fractionation techniques. In this report we analyze the macromolecular composition of isolated *Spisula* nucleolini and examine the relationship of this structure to the nucleolus and cell division apparatus. Analysis of nucleolinar RNA and protein revealed a set of molecules that overlaps with, but is nevertheless distinct from the nucleolus. The proteins identified were primarily ones involved in nucleic acid metabolism and cell cycle regulation. Monoclonal antibodies generated against isolated nucleolini revealed centrosomal forerunners in the oocyte cytoplasm. Finally, induction of damage to the nucleolinus by laser microsurgery altered the trafficking of α- and γ-tubulin after fertilization. These observations strongly support a role for the nucleolinus in cell division and represent our first clues regarding mechanism.

The nucleolinus (NLi)[1] is a compartment or organelle described in a wide variety of

cells and with a long, though virtually forgotten history (2,3). In cells where it is clearly visible it is closely apposed to the nucleolus, and in other cells where it has been described it appears to be integrated within the nucleolus. In the latter case, visualization of the NLi was achieved by innovative histochemical techniques (4,5). Given that generalized histochemical stains are rarely used nowadays in fundamental cell biology research, let alone the special preparations required for the NLi, it is not so surprising that studies on this compartment are few and far between.

With the existing lack of information, we cannot even be certain if the entities described by earlier investigators under the name of NLi are actually analogous structures in the various experimental systems used. Other than to say it contains RNA and protein (6), we know virtually nothing of its composition and have no molecular probes (until very recently) with which to study its biogenesis or behavior. By default, the NLi has been considered a part of the nucleolus by the few investigators who are even moderately familiar with it. In his landmark treatise on the nucleolus, Montgomery (7) stated, "I can attach no particular morphological significance to the nucleolinus; it appears to be only a detached portion of the nucleolar ground substance". Yet, there are indications that the NLi can and should be considered a distinct cellular compartment. These include the observations that in some cells, particularly invertebrate oocytes, it is morphologically distinct (7-9). Moreover, in cells where it is not visible by unaided brightfield microscopy, histochemical stains clearly differentiate it from the nucleolus and other cellular compartments (4,10). Finally, its behaviour under certain physiological conditions, such as during viral infection, serum starvation, and fertilization of invertebrate oocytes, distinguish it physically from the closely allied nucleolus (11-13). A reasonable operational definition for the NLi may therefore be a cellular compartment closely associated with the nucleolus that can be physically differentiated from the latter by histochemical means and under certain physiological conditions.

It has long been thought that the NLi is associated with the cell division apparatus (9,11,14,15), either as a precursor to centrosomes or in some other way contributing to spindle formation. This has recently been confirmed in surf clam (*Spisula*) oocytes (2). In these cells, centrosomes form "*de novo*" several minutes after fertilization or parthenogenetic activation (16). Induction of damage to the NLi via laser microsurgery before centrosomes or asters develop resulted in a malformed meiotic spindle and failed chromatin segregation in parthenogenetically activated oocytes. γ-tubulin immunofluorescence suggested that centrosomes could form, but their appearance and number may have been disregulated. In oocytes fertilized with sperm after microsurgery, mitotic centrosomes and the spindle failed to form altogether. Although it was considered unlikely that the NLi is a direct precursor of centrosomes as suggested by Lavdowsky (14), it was clear that the NLi plays a role in spindle morphogensis.

These observations are timely in light of data indicating the plurifunctional nature of the nucleolus and, in particular, its direct role in cell cycle regulation (17-20). The NLi is on one hand demonstrably associated with cell division (2,3) and on the other hand, as noted above, is intimately associated with the nucleolus. This gives rise to a number of questions regarding the interplay between the two and their respective physiolgical roles. Do the nucleolus and NLi act in concert to affect cell division? How are they related in their protein and RNA composition — should they be considered separate compartments?

The *Spisula* oocyte provides a unique system to observe the interaction between these fundamental structures. The nucleolus and NLi stand out in clear relief using brightfield optics within the large oocyte nucleus (germinal vesicle; GV). Centrosomes and other microtubule assemblages are not present in unactivated oocytes (16), but their

"*de novo*" formation can be induced by fertilization or parthenogenetic activation. Taking advantage of these characteristics, our aims in this study were to determine the composition of the *Spisula* Nli, develop specific probes to study its dynamics, and explore its ties to the nucleolus and cell division apparatus. Evidence is provided that, despite an intimate association with the nucleolus, the NLi contains a distinct set of molecules. mcAb to one of these components reveal a centrosomal forerunner in the cytoplasm, and perturbation of the NLi via laser microsurgery suggests a role in tubulin recruitment to the forming cell division apparatus.

Experimental Procedures

Gravid *Spisula solidissima* were obtained from the Marine Resources Center at the Marine Biological Laboratory, Woods Hole, MA. Gametes were collected by dissection. Oocytes were rinsed several times in 0.45µm filtered sea water and fertilized with sperm (diluted 1/20,000) in Tris-buffered (pH 8.0), filtered sea water. All brightfield and immunofluorescence imaging was performed with a Nikon 90i microscope equipped with DIC, epifluorescence, and a Photometrics CoolSNAP EZ digital camera. Immunofluorescence was performed, with minor modifications, as described in an earlier report (2). To visualize centrosomes and avoid cross-talk between secondary antibodies, anti-γ-tubulin IgG was directly conjugated to Alexafluor-594. Every immunofluorescent experiment was accompanied by a battery of controls for antibody specificity, cross-reactivity, and fluorophore channel overlap.

Isolation of nucleolini

Nucleolini are isolated in a two-step process. The first step is isolation of GVs based on methods described by Maul and Avdalovic (21). Starting with 8-10mL of packed, unactivated oocytes distributed between four 50mL conical centrifuge tubes, the cells are resuspended by addition of 20mL of buffer containing 1M glycerol and 20mM sodium phosphate, pH 8.0, incubated at room temperature for three minutes, and sedimented at 1,750xg for 15 seconds. The oocytes are resuspended to 40mL in ice cold lysis buffer (0.5M hexylene glycol, 0.75mM $MgCl_2$, 1mM HEPES, pH 7.5) with occasional mixing by inversion. They are incubated at room temperature and monitored by phase contrast microscopy every 2-3 minutes until all cellular structure is dissolved, leaving only intact GVs. The nucleolus dissolves during the lysis step. Nuclear envelopes are stabilized by addition of 8mL ice cold 40% sucrose with gentle mixing, and the tubes are placed on ice. The lysate is centrifuged at 780xg for 8 minutes (4°C) through a 2.0mL cushion of 10% sucrose buffer (1:1 lysis buffer:20% sucrose) in a swinging bucket rotor. The pellet is frozen in liquid nitrogen and stored at -80°C for later use. Only three structural elements are visible by DIC microscopy in these isolated GV preparations: the nuclear envelope with attached chromosomes, and the NLi.

Nucleolini are harvested from this preparation in the second step. One mL of frozen GVs are thawed on ice and resuspended with 5mL 10% sucrose buffer. GVs are disrupted by sonication on ice with three bursts of eight seconds each at 11W with a microprobe sonicator. Samples were then underlain with 2mL 40% sucrose (w/v) in 0.5M hexylene glycol, 0.75mM $MgCl_2$, and 1mM HEPES, pH 7.5, and centrifuged for 10 minutes at 500xg. The pellet is washed twice by sedimentation and resuspension in ice cold PBS in a microcentrifuge for one minute at maximum speed. For estimates of RNA and protein content, NLi were counted using a hemocytometer, RNA was estimated by $Abs_{280/260/230}$, and protein was determined using Pierce BCA assay reagents.

Characterization of nucleolinar RNA

RNA was extracted from isolated NLi using Qiagen RNeasy reagents, reverse transcribed using universal primers described previously (22), and blunt-cloned into

Invitrogen PCR-script plasmid. To guard against the potential amplification and subsequent cloning of genomic DNA contaminants, equal quantities of non-reverse transcribed NLi RNA were used as a control template. Non-reverse transcribed NLi RNA yielded no detectable products from random PCR nor, subsequently, cloned inserts. More than 3,000 clones were sequenced by the Sanger method. Ribosomal RNA was filtered from the pool in an initial BLASTn analysis leaving approximately 10% of the sequences for additional analysis.

Methods for *in situ* hybridization were described in an earlier report (2). The protocol was optimized to conserve nucleolar and NLi morphology (both of which are labile) throughout the hybridization regimen, as well as γ-tubulin antigenicity. *In situ* hybridization conditions could not be found that preserved the antigenicity of β-tubulin. Samples were hybridized with digoxygenin-labeled NLi RNA probes for 2 days at 58-60°C. Alkaline phosphatase reaction product was visualized after development at 4°C with gentle rocking. Specificity controls for *in situ* hybridization included opposite strand ("sense") hybridizations and comparison of labeling pattern with other RNA probes.

Analysis of NLi Proteins

Reagents: MS-grade solvents were from Burdick and Jackson, or Baker. Sequencing grade trypsin was from Promega. Other solutions were the highest grade available from Sigma-Aldrich.

Digestion: For solution digests, the protein sample was dissolved in 8 M urea, 5 mM tris(2-carboxyethyl) phosphine, 100 mM Tris-HCL pH = 8.5 for 40 minutes at room temperature. After incubation, 1/20th volume of 200 mM iodoacetamide was added, and the alkylation was allowed to proceed for 15 min in the dark at room temperature. The sample was then diluted with three volumes of 100 mM Tris-HCL pH 8.5, and digested with 4 μg/ml trypsin overnight at 37°C. Digested samples were purified with C18 affinity tips following the manufacturer's recommendations (Agilent Technologies), redissolved in 1% formic acid, and analyzed by LC-MS/MS as described below.

LC-MS/MS Methodology: Samples were analyzed on a hybrid LTQ-Orbitrap mass spectrometer (Thermo Fisher Scientific) coupled to a New Objectives PV-550 nanoelectrospray ion source and an Eksigent NanoLC-2D chromatography system. Peptides were trapped on a 150μm id x 2.5-cm pre-column, and separated on a 75μm id x 15-cm length analytical column terminated with an integral fused silica emitter pulled in house. Both columns were packed in house with Magic C18 AQ, and plumbed in a vented column configuration. Peptides were eluted using a 2.5-28% ACN/0.1% formic acid gradient performed over 42 min at a flow rate of 300 nL/min.

During each scan cycle, one full-range FT-MS scan (nominal resolution of 60,000 FWHM, 360 to 1400 m/z) was collected, whilst the six most intense ions were analyzed via MS/MS in the linear ion trap. Data dependent MS/MS settings used a trigger threshold of 8,000 counts and monoisotopic precursor selection (MIPS). Ions previously selected for MS/MS were dynamically excluded for a duration corresponding to 150% of the observed chromatographic peak width, and using an exclusion count of two. Ions whose charge states could not be assigned were also excluded from MS/MS. Ions that were previously identified as contaminants on blank gradient runs were also excluded.

For mass spectrometry analysis, centroided ion masses were extracted using the extract_msn.exe utility from Bioworks 3.3.1 and were used for database searching with Mascot v2.2.04 (Matrix Science) and X! Tandem v2007.01.01.1 (www.thegpm.org). Searches were conducted using the following search parameters: parent mass tolerance 5 ppm, fragment mass tolerance 0.8 Da, one missed tryptic cleavage, and peptide modifications pyroglutamate cyclization of N-terminal Gln, oxidation of Met, formylation or

acetylation of the protein N-terminus, alkylation of Cys by iodoacetamide. The database search utilized a local copy of NCBInr that was downloaded on 03/28/10 and contained 10,810,288 protein sequence entries. Searches were also conducted using a reversed-sequence decoy strategy. A species filter was not used. Peptide and protein identifications were validated using Scaffold v2.2.00 (Proteome Software) and the PeptideProphet algorithm (23). Probability thresholds were greater than 99% probability for protein identifications, based upon at least 2 individual peptides, each identified with 95% probability. Proteins that contained similar peptides and could not be differentiated based on MS/MS analysis alone were grouped to satisfy the principles of parsimony. To confirm the identities of individual key peptides from the proteins fibrillarin, Nop2, Cdk1, and Nop56, experimental MS/MS spectra identifying peptides from these proteins were compared to archived MS/MS spectra from Peptide Atlas (http://www.peptideatlas.org/publications.php) To quantitate peptide abundances, ion-specific chromatograms for each peptide were extracted to the second decimal place and their peak areas measured using QuantBrowser (Thermo). To verify each ion peak, the elution times of these extracted ion peaks were compared to the elution time at which each identifying MS/MS spectra was collected.

The immunization regimen and generation of hybridoma cells to produce mcAbs against isolated NLi were performed by Cell Essentials, Inc. (Boston). Hybridomas were screened to select positive clones by ELISA and subsequently immunofluorescence microscopy and western blot.

Laser Microsurgery

For laser microsurgery, 8-10 oocytes were transferred into a 3µL drop of 0.45µm-buffered sea water in a Hamilton Thorne 2X-CEL 80µm Analysis Chamber. The chamber was closed with a 2X-CEL coverslip and topped with a 1.0mm thick glass cover. A 150µs pulsed 1480nm laser set at 300mW was directed into a 5µm spot through the 40x objective using a Hamilton Thorne (Beverly, MA) XYClone laser system mounted on a Nikon 90i microscope. A visible lightbeam sight guide of the same diameter was used to effect precise targeting. Controls were irradiated using these same parameters, but instead striking within the nucleolus. Following irradiation, oocytes were quickly transferred to fresh sea water and fertilized. Oocytes were fixed at 10 minutes post-fertilization to visualize the NLi, centrosomes, and asters by immunofluorescence. We reiterate here for clarity that at the time of laser irradiation (unactivated oocyte stage), no centrosomes or spindle are present. These elements arise only *after* fertilization or parthenogenetic activation.

Results

RNA content of the NLi

NLi can be separated from nucleoli and other cell components by sucrose density gradient centrifugation for compositional analysis. First, GVs are isolated from unactivated oocytes based on methods described by Maul and Avdalovic (21). This step eliminates almost all cellular debris (Fig. 1A-C). Nucleoli are highly labile and disintegrate during cell lysis (Fig. 1B), leaving only three structures visible in the preparation: the nuclear envelope, and the prophase chromosomes and NLi within (Fig. 1C). NLi are highly dense and are separated from nuclear envelopes, chromatin, and soluble contaminants by sonication and centrifugation through 40% sucrose at just 780xg for 8 minutes (Fig. 1D). In addition to monitoring the enrichment of NLi during cell fractionation by DIC microscopy (Fig. 1), LC-MS/MS and western blots were used to assess the enrichment of specific NLi components (described in detail in subsequent sections of this report) .

Total RNA was extracted from isolated NLi for library construction and sequence analysis. We estimated 0.7 ± 0.16 (SEM) pg of RNA per NLi. An initial BLAST analysis

revealed that ribosomal RNA sequences constituted approximately 91% of our clones. These were screened out of our sample set. Cloning and sequencing was continued until the library was deemed exhausted of new non-rRNA sequences, a point reached after approximately 3,100 cDNA clones. A total of 266 non-rRNAs were identified for subsequent analysis (Supplemental Table 1), all but three found among the first 1,800 clones sequenced. Although it cannot be quantitated at present, this suggests that the resident transcriptome of the NLi is substantially limited in scope.

The major component of the NLi RNA library, comprising approximately 67% of clones, assembled into a single 1.1kb contig, named Contig 1. Contig 1 included the NLi-1 sequence previously reported to localize specifically to the NLi by *in situ* hybridization (2) . The remaining 89 (non-Contig 1) sequences included 37 independent clones and 52 others that assembled into 16 contigs for a total of 54 unique, non-rRNA sequences (Genbank accession numbers JN196042 - JN196094). These ranged in size from 41 to 415nt in length. Thirteen of these exhibited similarity to database entries, most at low stringency (Table 1). Noteworthy examples include clone N11E09, which exhibited similarity ($8e^{-16}$) to centrosome-associated RNA from *Spisula*; clone N27B08, similar to a *Spisula* zinc finger protein ($2e^{-27}$) also found associated with centrosomes (22); and clone N2C05, which exhibited high identity ($2e^{-73}$) with an uncharacterized human chromosomal segment. In addition to NLi-1 RNA, three other sequences (Contig 2, N2C05, and N3H05) were examined by *in situ* hybridization. All three were localized to the NLi in unactivated oocytes (Fig. 2) and until a more descriptive name is determined, are referred to as NLi-2 through NLi-4 RNAs, respectively.

Protein components of the NLi

We measured 5 ± 1.7 (SEM) pg of protein per nucleolinus, indicating a mass ratio of protein:RNA of seven. Coomassie-stained SDS gels of proteins isolated with NLi revealed six major polypeptide bands (76kDa, 66kDa, 65kDa, 63kDa, 39kDa, and 33kDa) among approximately 50 minor bands. The great majority of these were significantly attenuated after treatment of preparations with 1M NaCl to strip molecules less stringently associated with the complex by ionic interaction (Fig. 3). The major bands were also greatly reduced with 1M NaCl, but remained among the more prominent protein components of the preparation. Four other polypeptides in the preparation appeared to be resistant to 1M NaCl treatment (indicated by arrowheads in Fig. 3), suggesting a tight association with NLi. An association via ionic interaction (i.e. sensitivity to 1M NaCl) does not preclude an integral and physiological association, however, NaCl-washed NLi were used for increased stringency in our initial MS analysis of NLi protein composition, described below.

NLi protein samples were analyzed by trypsinolysis, liquid chromatography, and tandem mass spectrometry (LC-MS/MS). Subsequently, the masses of experimental peptides and peptide fragments were compared to those predicted from a database of protein sequences. Only 48 *Spisula solidissima* protein sequences were available in NCBInr. Thus, we utilized the whole NCBInr database as a proxy for the *S. solidissima* proteome, searching for cross-species peptide matches to interpret our experimental MS/MS data. We used several approaches to minimize the impact of random matches between our experimental data and the large number of peptides predicted by NCBInr sequence (see *Experimental Procedures*). The goal of these strategies was not to maximize the number of proteins identified, but rather to generate a short list of high-confidence protein identifications. This strategy generated a short list of 24 candidate protein identifications. Each of these proteins was identified on the basis of 2 to 6 unique peptides covering 1.2% to 25% of protein's sequence. As might be expected from our high-stringency statistical filters, our short list of proteins did not include any decoy (reversed) peptide or protein sequences (i.e

our false discovery rate was zero). A chromatographic blank run immediately prior to the NLi sample testified that these peptides were specific to the NLi sample. Several human skin keratin proteins were also identified, but were judged to be contaminants. For hypothetical NCBInr proteins lacking meaningful annotation, the candidate protein sequence was further analyzed by BLAST searching against SwissProt.

The identities of the NLi protein candidates were highly consistent with their identification as components of NLi preparations (Table 2 and Supplemental Table 2). Among the 24 proteins identified, 20 were predicted to localize to the nucleus. Among these 20 were seven with a predicted dual localization, including ribosomal/pre-ribosomal components and peroxyredoxin. We include actin 1g in this number. Although the presence of actin in the nucleus is considered controversial by some and its function is a matter of debate, there are increasing numbers of reports on actin and actin-binding proteins in the nucleus (24-26). Also represented were a Ras-related protein (Rab7) that regulates vesicle trafficking, and a subunit of mitochondrial ATP synthase. Eighteen of the 24 proteins identified are involved with RNA/DNA conformation and metabolism; helicases, methylases, etc. The fact that the proteins we identified were thematically consistent with our biological sample argued that the individual protein identifications presented in Table 2 are valid. The proteins' identities themelves suggest that NLi are sites of RNA processing and maturation *in vivo*. Moreover, since half of the 24 proteins identified, such as Cdk1, RuvB, Serine/arginine-rich splicing factors 1 and 6, BiP, elongation factor 1α, and DEAD box RNA helicase, are required for cell cycle progression, the data support a role for the NLi in cell cycle control.

To gain additional insight into the protein composition of NLi, we repeated our LC-MS/MS analysis, characterizing equal µg-amounts from four key fractions in purification scheme (unactivated oocytes, first 10% sucrose pellet, isolated GVs, and final NLi pellet) and quantifying the chromatographic peak areas of each peptide. We observed three peptide behaviors (Supplemental Table 3) in this analysis. The first includes peptides showing no enrichment. These most likely represent contaminant proteins or, at any rate, cannot be assigned to the NLi with confidence. The second group includes peptides that were enriched at each stage but were attenuated in the final high stringency (1M NaCl) wash. This group most likely represents proteins associated with the NLi, but probably by ionic interactions. The third group of peptides, including fibrillarin, two isoforms of Nop56, Nop2, and Cdk1, were enriched throughout the procedure, indicating they are tightly associated with the NLi (Fig. 4). In addition to these, *Spisula* nucleolinin (described below) was tracked in the same series of cell fractions and was found to be substantially enriched in western blots (Supplemental Fig. 1).

Because the *Spisula* genome was not available to support searching against our MS/MS data, it was necessary to use the whole NCBInr database as a proxy for the *Spisula* proteome. This implied a degree of uncertainty regarding each peptide identification, despite the strong Mascot and Xtandem! scores that we obtained and the stringent statistical filters to which they were subjected. To address remaining uncertainties, we searched Peptide Atlas for previously identified fibrillarin, Nop56, Nop2, and Cdk1 peptides. Peptide Atlas is a database of *bona fide* peptide MS/MS spectra, and each entry displays the characteristic experimental MS/MS fragmentation patterns of the peptides documented therein. We noted near-perfect agreement between our *Spisula* MS/MS spectra and those appearing in Peptide Atlas, with each peptide's fragment ion masses and the fragments' relative ion intensities being highly conserved between both sets of spectra (Supplemental Fig. 2). Thus, each of the *Spisula* peptides were unambiguously identified and, by extension, this supported the identification of their parent proteins.

To acquire immunological probes recognizing protein components of the NLi, hybridomas were developed using isolated NLi as immunogen. ELISA-positive clones were subsequently screened by immunofluorescence in unactivated oocytes to select those labeling NLi *in situ*. Three anti-NLi hybridoma cell lines were identified, all apparently producing antibody to the same dominant antigen, because all three yielded the same immunofluorescent labeling pattern and recognized the same polypeptide band(s) on western blots at approximately 33kDa (Fig. 5A). Until an identification is made, this antigen is referred to as nucleolinin. A faintly stained band at over 60kDa was also observed. We believe this represents a minor dimerization product, based on gels run in the absence of dithiothreitol. One antibody (McAb23) exhibited a slightly greater signal intensity than the other two and was therefore used for the purposes of this study. Immunofluorescent labeling for nucleolinin appeared as an elongate or crescent-shaped patch at the apical pole [1] of the NLi (Fig. 5B-D). In approximately one-third of cases, this NLi staining was accompanied by a single punctum in the cytoplasm. The oocyte depicted in Fig. 5 was selected to illustrate this. The cytoplasmic punctum was often in contact with, or in close apposition to, the apical pole crescent, giving the impression that it was fixed in the process of budding.

Links between the NLi and cell division apparatus

We followed the fate of the nucleolinin during meiosis. The expression pattern was complex and dynamic. Whether or not, as described above, the cytoplasm of unactivated oocytes contained one nucleolinin punctum, within three minutes after fertilization two such puncta were present. Again, proximity to and contact with the NLi at early time points gave the appearance of budding (Fig. 6). The next event noted was that one, and then both cytoplasmic puncta became positive for γ-tubulin. The recruitment of γ-tubulin to these nucleolinin foci identifies them as forerunners of the meiotic centrosomes. During this time (four to eight minutes post-insemination), staining in the area of the apical pole was observed to spread across the NLi. Nucleolinin immunoreactivity is subsequently lost from one, then both centrosomes, and finally from the NLi itself, although an immunofluorescent patch persists for approximately two minutes beyond the time when the NLi is visible by DIC. Nucleolinin does not slowly disperse (see Fig. 6 F-J for comparison), but appears to be rapidly downregulated. Observations on the association of NLi-RNA with centrosomes and the spindle (2) taken together with these immunofluorescent images of an antigen shared between the NLi and newly forming centrosomes provide direct evidence for compositional links between this nuclear compartment (the NLi) and the cell division apparatus.

A functional link between the NLi and cell division apparatus is supported by earlier experiments in which laser-induced damage to the NLi resulted in aborted cell division (2). However, little could be asserted regarding the etiology of the accompanying malformed spindle. In the experiment to be described next, the use of mcAb23 to nucleolinin enabled us to monitor certain early events following microsurgery. Sixteen unactivated oocytes were subjected to laser microsurgery; an experimental group of eight targeting the NLi, and a control group of eight targeting the nucleolus. These oocytes were then fertilized, fixed at 10 minutes, and labeled for nucleolinin, β- and γ-tubulin. Significant differences were noted between the experimental and control groups. First and foremost, 0/8 NLi-targeted oocytes formed asters, while asters were formed in 7/8 controls. In the experimental group, nucleolinin staining could still be observed in 7/8 oocytes. In all of these seven, β- and γ-tubulins were heavily recruited to the site of the NLi (Fig. 7A-C). Similar to our

[1] For descriptive purposes, we will refer to the point of contact between the edge of the NLi, nucleolus, and GV as the apical pole.

observations reported previously (2), γ-tubulin-positive foci (centrosomes) were present, although these sometimes appeared diminutive and/or fragmented (Fig. 7D). In the one remaining experimental case (Fig. 7E-G), nucleolinin staining was completely abolished. The tubulins were concentrated together in a single, nucleolinin-negative patch in this oocyte, and no centrosomes were present. In the control group of eight oocytes (targeted on the nucleolus), the seven that showed no abnormal recruitment of β- and γ-tubulin to the NLi were the same seven that formed asters (Fig. 7H-J). Abnormal recruitment was observed in one case, and it was this one oocyte demonstrating a malformed aster. The results suggest that the NLi or elements derived from the NLi play a role in β- and γ-tubulin recruitment during normal spindle morphogenesis. Perturbation of the NLi by laser microsurgery led to their mislocalization.

Interplay between the NLi and nucleolus

If not a full-fledged continuum between the nucleolus, NLi, and division apparatus, then at least serial physiological links must exist between the three. Establishing a relationship has been hampered by their transient nature as well as a lack of specific probes for what is the likely middlepiece of the trio, the NLi. However, we are now able to visualize morphological overlaps. As was the case for the formation of centrosomal forerunners expressing Nli protein described above, the interplay between the nucleolus and NLi is complicated both temporally and spatially. At first the NLi and nucleolus are present at the same time and in close apposition to one another. Then, at approximately four minutes post-insemination, the nucleolus begins to dissipate. Rather than a simple dissipation as has been frequently described (27), nucleolar disassembly in *Spisula* oocytes is characterized by an apparent incorporation into the NLi (Fig. 8 and Supplemental Video 1). Except for localized oscillations, the NLi typically remains in its original position. The nucleolus, while appearing to be tethered to the apical pole of the NLi, collapses into the latter. The overall appearance is that of a balloon held by its neck while being steadlily deflated.

These observations highlight the close interplay between the nucleolus and NLi, but do not disclose the fate of nucleolar contents. This question was addressed using mcAb53 which specifically recognizes components of the *Spisula* nucleolus. Rather than a gradual flow of signal into the NLi as DIC images would suggest, nucleolar contents were left behind during this recoil and dispersed throughout the GV (Fig. 9A-F). Then, after being clearly excluded for the first 8-10 minutes after fertilization, diffuse mcAb53 staining subsequently appears in the NLi (Fig. 9G, H). The mcAb53 patch condenses into a distinct focal point that remains after the NLi has itself dissipated (Fig. 9I-L). These and other events related to NLi dynamics are summarized in Fig. 10. We do not know whether an analogous process occurs in cells without a morphologically distinct Nli, but these images in *Spisula* oocytes provide a unique view of nucleolar-NLi interaction and dynamics.

Discussion

On the nucleolinus

Many of the cellular compartments, inclusions, and organelles we study today were discovered over 100 years ago. As we learn more about the composition of a given complex and the forms it takes in different cell types, the terminology associated with it may be modified or altogether abandoned. We allow that this may be the case for the NLi. For example, the NLi could have been "forgotten" because it was redefined as one of the (now) well characterized nucleolar subcompartments (fibrillar center, dense fibrillar component, granular component). However, at least three observations suggest the solution is not that simple. First, we can find nothing in the literature linking the term "nucleolinus" to a revised descriptor associated with the nucleolus or any other

nuclear structures, such as Cajal bodies, PML bodies, and histone locus bodies. Second, the NLi differs morphologically from any of these others, being 5- to 10-fold larger. Third is preliminary immunological evidence. The *Drosophila* nucleolus contains a mcAb23-reactive antigen (nucleolinin), but Cajal, PML, and histone locus bodies are all mcAb23-negative, and antibodies to the Cajal body protein, pigpen (28) do not stain the *Spisula* NLi (unpublished observations). A lack of immunoreactivity between species does not rule out a relationship to these other nuclear bodies. However, there is no evidence to suggest their equivalence.

Perhaps the NLi is related to the perinucleolar compartment found predominently in cancer cells (29) or the intranucleolar bodies associated with rDNA described recently in HeLa and other mammalian cells (30). In the latter case, immunological probes were used to show the compartment exhibits compositional overlap with the nucleolus but is nevertheless distinct from the three most widely recognized nucleolar subcompartments. Moreover, FRAP was used to show the dynamic nature of rDNA-associated intranculeolar bodies and their exchange of proteins — in some cases very rapid — with other nucleolar subcompartments. rDNA-associated intranucleolar bodies are notable for other reasons with respect to the NLi in that they are sometimes visible with DIC optics and are enriched in, among other things, proteins involved in RNA processing and chromatin organization. Finally, it must be considered that structures described by investigators over the past 150 years as NLi are not at all analogous to one another, but mistakenly collected under the same moniker for lack of better information. With so little data available on the composition, dynamics, and function of the NLi, it is simply not feasible to discriminate between the possibilities.

Until recently, we knew only that the NLi was comprised of RNA and protein (6). No information was available on specific molecules. The present study does not purport to establish the complete proteome nor complete resident transcriptome of this structure, but provides significant new compositional data. BLAST analysis of the several dozen RNAs extracted from isolated NLi resulted in few database matches, and almost all of these were to minimally characterized entries. The exceptions included two sequences isolated with *Spisula* centrosomes in an earlier study (22) and the mRNA encoding a zinc finger protein. With the exception of NLi-1, NLi RNA is composed largely of small sequences. It is possible we have not yet uncovered overlapping sequences to unite the small ones into longer contigs. However, we think this unlikely because the 17 contigs that are part of our data set are only nominally longer than the independent clones (120 vs. 115nt in length, respectively). The presence of small RNAs and characterized microRNAs in the mammalian nucleolus (31) also suggest our findings may truly reflect the size range of these NLi RNAs. However, we cannot be certain until an exhaustive sequencing and assembly effort has been undertaken.

A stringent interpretation of LC-MS data on NLi proteins yielded a set of 24 proteins identified with high confidence. These were primarily well characterized components of RNP complexes involved in polynucleotide biochemistry (structural conformation, metabolism) and cell cycle regulation. A number of these, such as the helicases, and RuvB in particular, fall into both categories. RuvB is an ATP-dependent helicase reported to interact with the γ-tubulin ring complex and exhibiting pleiotropic effects on spindle formation (32). Comparison of experimental MS/MS spectra derived from various cell fractions to archived MS/MS spectra from Peptide Atlas allows us to conclude with certainty that Cdk1, Nop2, fibrillarin, and two isoforms of Nop56 are intimate components of *Spisula* NLi. As with our analysis of NLi-derived RNA, this collection of proteins does not represent a comprehensive set, i.e. a NLi proteome, and their presence in the NLi must yet be confirmed *in situ*. However, it does represent the first evidence associating any

specific proteins with this little known cellular compartment. The significant presence of cell cycle regulators, together with the observations discussed below, are a solid starting point for the development of functional hypotheses.

Interplay between the nucleolus, NLi, and cell division apparatus

Several other investigators have posited that the NLi is intimately related to the cell division apparatus. Lavdowski [quoted in (7)] hypothesized that the NLi represented the centrosomes in the process of formation, although as Montgomery (7) points out, he was not able to demonstrate the steps by which this process occurred. Support for Lavdowksi's position (at least in part) may have come much later, in electron microscopic and fluorescence studies indicating the formation of MTOCs derived from nuclear RNP in slime mold (*Physarum*) plasmodia (33,34). Allen (9) concluded, but did not present any supporting evidence, that the NLi is involved in spindle formation, and Love and Wildy (11) reported events in mitosis corresponding with NLi physiology in transformed and virally infected mammalian cells. These suggestions and others going back more than 100 years may have been prescient, but were based on correlative evidence only. Experimental data showing a relationship between the NLi and cell division apparatus has only recently been recorded (2). The present study begins to outline the mechanisms involved. The NLi appears to participate in the formation of centrosomes and, based on the results of our laser microsurgery experiment, may play a role in the recruitment of tubulins.

The intimate relationship between the nucleolus and NLi in these oocytes as seen by DIC and with new molecular markers provides the first morphological links between these two structures and the cell division apparatus. Whether or not the NLi is a separate compartment in most cell types, it may at least represent that component of the nucleolus responsible for cell cycle functions. Moreover, the use of mcAb23 to monitor the distribution of nucleolinin in unfertilized oocytes may help provide an explanation of why laser microsurgery had such profound effects on spindle morphogenesis but appeared to have minimal effects on centrosomes (2). In approximately one-third of unfertilized oocytes, one procentrosome was already present in the cytoplasm (Fig. 5). This nucleolinin-postive structure would therefore have escaped laser treatment and could later recruit γ-tubulin, but was probably not fully competent as a MTOC. Our increased knowledge of NLi composition, an ability to examine its presence and behavior in other cell types, and the development of new functional probes will make it possible to piece together this and other puzzles. For the present, we are able to refine our definition of the NLi to reflect it's distinct molecular composition and demonstrated association with centrosomes and the spindle.

References

1. Agassiz, L. (1857) First Monograph. Part IIL *Embryology of the Turtle*. Boston.
2. Alliegro, M.A., Henry J., and Alliegro M.C. (2010) *Proc. Nat'l Acad Sci USA*, **107,** 13718-13723.
3. Alliegro M.C. (2011) *Comm. Int. Biol.* **4,** 147-149..
4. Carleton, H.M. (1920) *Quart. J. Microsc. Sci.* **s2-64,** 329-341.
5. Love, R. and Liles, R.H. (1959) *J. Histochem. Cytochem.* **7,** 164-181.
6. Love, R. and Walsh, R.J. (1968) *Cancer Res.* **30,** 990-997.
7. Montgomery, T.H. (1898) *J. Morph.* **15,** 265.
8. Gates, R.R. (1942) *Biol. Bull.* **82,** 47-51.
9. Allen, R.D. (1953) *Biol. Bull.* **105,** 213-239.
10. Love, R. and Bharadwaj, T.P. (1959) *Nature* **183,** 1453-1454.

11. Love, R. and Wildy, P. (1963) *J. Cell Biol.* **17,** 237-254.
12. Love, R. (1966) *Nat'l. Cancer Inst. Monographs* **23,** 167-180.
13. Mironescue, S., Encut, I., Mironescu, K., and Liciu, F. (1968) *J. Nat'l. Cancer Inst.* **40,** 917-933.
14. Lavdowsky, M. (1894) *Zellen. Merkel und Bonnefs Anat.* Hefte.
15. Allen, R.D. (1951) *Biol. Bull.* **101,** 214.
16. Palazzo, R.E., Vaisberg, E., Cole, R.W., and Rieder, C.L. (1992) *Science* **256,** 219-221.
17. Gaulden, M.E. and Perry, R.P. (1958) *Proc. Nat'l. Acad. Sci. U.S.A.* **44,** 553-559.
18. Weber, J.D., Taylor, L.J., Roussel, M.F., Sherr, C.J., and Bar-Sagi, D. (1999) *Nature Cell Biol.* **1,** 20-26.
19. Ugrinova, I. *et al.* (2007) *BMC Mol. Biol.* **8,** 66.
20. Pederson T. (2011) *Cold Spring Harb Perspect Biol.* **3,** 1-15.
21. Maul, G.G. & Avdalovic, N. (1980) *Exp. Cell Res.* **130,** 229-240.
22. Alliegro, M.C. and Alliegro, M.A. (2008) *Proc. Nat'l. Acad. Sci. U.S.A.* **105,** 6993-6997.
23. Keller, A., Nesvizhskii, A., and Aebersold, R. (2002) *Anal. Chem.* **74,** 5383-5392.
24. Hoffman, W.A. (2009) *Int. Rev. Cell Mol. Biol.* **273,** 219-263.
25. Goyal, P., Behring, A., Kumar, A., and Siess, W. (2011) *PLoS One* 6:e16249.
26. Fenn, S., Breitsprecher, D., Gerhold, C.B., Witte, G., and Hopfner, K.P. (2011) *Embo J.* 30:2153-2166.
27. Alberts, B., Johnson, A., Lewis, J., Raff, M., Roberts, K., and Walter, P. (2008) *Molecular Biology of the Cell*, 5th Ed., Garland Science, New York, New York
28. Alliegro, M.C., and Alliegro, M.A. (1997) *Exp. Cell Res.* **231,** 373-377.
29. Pollock, C. and Huang, S. (2009) *J. Cell Biochem.* **107,** 189-193.
30. Hutten, S., Prescott, A., James, J., Reisenberg, S., Boulon, S., Lam, Y.W., and Lamond, A.J. (2011) *Chromosoma* 120:481-499.
31. Politz, J., Hogan, E.M. and Pederson, T. (2009) *RNA* **15,** 1705-1715.
32. Huen, J., Kakihara, Y., Ugwu, F., Cheung, K., Ortega, J., and Houry, W. (2010) *Biochem. Cell Biol.* **88,** 29-40.
33. Tanaka, K. (1973) *J. Cell Biol.* **57,** 220-224.
34. Laane M.M., and Haugli F.B. (1974) *Nor. J. Botany* **21,** 309-318.

Acknowledgments — This work was supported by a grant from the NIH (GM088503) to M.C.A. Mass spectrometry analyses were performed in the DNA/Protein Resource Facility at Oklahoma State University, using resources supported by the NSF MRI and EPSCoR programs (award #0722494 to S.D.H.). The authors are indebted to Lily Reed, Alex Ziolkowski, and Hamilton Thorne Biosciences for the loan of a XYClone laser system, without which functional studies would not have been possible.

FOOTNOTES

[1] Abbreviations used: NLi: nucleolinus, nucleolini, nucleolinar; MTOC: microtubule organizing center; mcAb: monoclonal antibody; DIC: differential interference contrast; LC: liquid chromatography; MS: mass spectrometry; BLAST: basic local alignment search tool; FRAP: fluorescence recovery after photobleaching.

[2] For descriptive purposes, we will refer to the point of contact between the edge of the NLi, nucleolus, and GV as the apical pole.

FIGURE LEGENDS

Figure 1. Isolation of nucleolini. A, intact, unactivated *Spisula* oocytes showing NLi (arrowhead) sitting atop spherical nucleoli (arrow), both lying within the large, tetraploid nucleus

(asterisk). B, oocytes in various stages of lysis; NLi and nuclei marked as in panel A. The nucleolus is labile and disintegrates early during lysis in glycerol-phosphate buffer, followed by dispersal of the oocyte surface and cytoplasm. C, After lysis and sucrose density gradient centrifugation to isolate nuclei, visible structures include chromosomes (white arrows) attached to the nuclear lamina, NLi (which become slightly more refractile and condensed during the procedure), and a small amount of debri. D, sonication to disrupt the intact nuclei followed by centrifugation through a cushion of 40% sucrose leaves a clean preparation of NLi. Size bar = 20μm.

Figure 2. Localization of RNAs extracted from isolated NLi. *In situ* hybridization showing localization of NLi-2 (Contig-1), NLi-3 (clone N2C05) and NLi-4 (clone N3H05) RNAs to the NLi (A-C, respectively). A full range of signal intensities is seen, likely due to a combination of target abundance and probe size (shorter sequence = less labeled precursor incorporation). In the case of NLi-4 (C), some reaction product is seen in the nucleoplasm immediately adjacent to the nucleolus, but controls using an opposite strand probe (D) suggest this nucleoplasmic staining is non-specific. Opposite strand controls for the other NLi RNAs were completely negative for the NLi (as exemplified in panel D) as well as the nucleoplasm. Cytpolasmic labeling was never observed. Arrowheads point to the NLi and arrows indicate the approximate borders of the nucleolus, which are less sharply demarcated after the three day hybridization regimen.

Figure 3. SDS polyacrylamide gel electrophoresis of isolated NLi proteins. At least six polypeptides stand out against a background of approximately 50 bands; 76kDa, 66kDa, 65kDa, 63kDa, 39kDa, and 33kDa. All of these were greatly diminished after washing the final NLi pellet with 1M NaCl. Four polypeptides in particular were resistent to the high-salt wash (arrowheads). Gel is 10% acrylamide. Positions of M_r standards marked with arrows on left.

Figure 4. Identification of specific NLi proteins by analysis of enrichment during cell fractionation. NLi were purified as described, and an equal amount of protein from each of four steps in the protocol was digested with trypsin and analyzed by LC-MS/MS. The indicated peptides and their protein parents were identified by database searching (see Methods). For each peptide, the peptide's ion-specific chromatogram was extracted and the area of its chromatographic peak measured. Peak areas were normalized to those observed in the final purified fraction, and represent the mean from three technical replicates +/- SEM. Key: gray shaded bars ( ), unactivated oocytes; left crosshatch ( ), first 10% sucrose pellet, as described in *Methods*; stipple ( ), isolated GVs; right crosshatch ( ), isolated NLi.

Figure 5. Immunofluorescence localization of nucleolinin in unactivated oocytes. A, immunoblot characterization of mcAb23 on whole cell lysate (50μg protein); left-hand lane coomassie blue-stained proteins, right-hand lane immunoblot. Control lane probed with P3x (parent myeloma) supernatant was negative (not shown). Positions of M_r standards are indicated to the left. The *in situ* localization pattern is shown in panels B-D. Antibody staining is observed on the "apical pole" of the NLi in a crescent configuration. Although atypical in unfertilized oocytes, this cell contains one cytoplasmic punctum as well. B, DIC image; C, nucleolinin; D, overlay.

Figure 6. Dynamics of nucleolinin expression during meiosis. Minutes post-fertilization are indicated across top row. Between 2 and 4 minutes, nucleolinin (NLn) originally present as a thin crescent, has begun to expand across the NLi (arrowhead). A single nucleolinin-positive punctum is present at 2 minutes which is originally γ-tubulin (-), but by 4 minutes is γ-tubulin(+). By 8 minutes, two nucleolinin foci are present, both γ-tubulin-positive. The intensity of γ-tubulin staining increases over time in centrosomes while nucleolinin signal disappears. Meanwhile, the

nucleolus has dissipated by 12 minutes leaving the NLi still clearly visible by DIC. Nucleolinin staining has expanded to its maximum. At 16 minutes the NLi is no longer visible by DIC but a strong nucleolinin fluorescent signal persists. Shortly thereafter (20 minutes post-fertilization), nucleolinin expression is gone even from the NLi. Anti-γ-tubulin staining of centrosomes remains strong and sharp.

Figure 7. Laser microsurgery on the unfertilized oocyte NLi results in mis-recruitment of tubulins. A, oocyte targeted on the NLi, fixed at 10 minutes post-insemination, and labeled with mcAb23 to mark the NLi (arrowhead). Panels B and C show the distribution of γ- and β-tubulin, respectively, in this same oocyte. Centrosomes may be present (arrow in B) but no asters are formed (C). Instead, γ- and β-tubulin accumulate at the NLi. Even though asters (and subsequently spindles) are either absent or malformed in such oocytes (1), effects on centrosomes as determined by anti-γ-tubulin immunofluorescence are difficult to detect. However, they sometimes appear smaller, more weakly labeled, fragmented, or supernumerary, as illustrated in the oocyte shown in panel D. In the oocyte shown in panel E, mcAb23 staining was completely ablated. In this case, γ- and β-tubulin form an aggregate in the peripheral cytoplasm (arrows in F,G). H, control oocyte (laser-targeted on the nucleolus) labeled with mcAb23. Centrosomes (I, arrows) and asters (J) are clearly developed and there is no untoward accumulation of γ- or β-tubulin at the NLi (position marked by arrowheads).

Figure 8. Time-lapse DIC series of nucleolar recoil into NLi. This series of images (selected frames from Supplemental Video 1) traces the disappearance of the nucleolus over the course of approximately 7 minutes following reinitiation of the cell cycle. For the first four minutes after cell cycle reinitiation, the nucleolus appears unchanged. Thereafter, it appears to "deflate" rapidly, collapsing like a tethered balloon into the NLi. White arrows in each panel mark the edge of the nucleolus during its recoil, and the the size and position of the nucleolus relative to the NLi from 4:20 to 11:20 are diagramed in the upper right hand corner of panel E. Size bar = 20μm.

Figure 9. Localization of nucleolar contents with mcAb53 and its relationship to the NLi and internal meiotic spindle pole. McAb53 is a specific marker for the nucleolus in *Spisula* oocytes. Paired DIC-immunofluorescent images are shown for an unactivated oocyte (A, B) and two minutes (C, D), four minutes (E, F), 10 minutes (G,H), and 12 minutes (I, J) post-insemination. The antigen is at first excluded from the NLi (A-F), but later accumulates there (G, H), condensing into a fine punctum (I, J). The mcAb53 focal point perists at the site of the NLi even after the latter is no longer visible by DIC. This is confirmed in 12 minute oocytes double-labeled for nucleolinin (K) and with mcAb53 (L). Arrowheads indicate the NLi, visualized either by DIC or immunofluorescence.

Figure 10. Spatial and temporal relationships between the nucleolus, nucleolinus, and centrosomes. Minutes post-fertilization (indicated across the top) are meant only as approximations because progress can vary depending on temperature, time of season, and between individual batches of gametes. The bulk of the cell mass is not depicted, only the nucleolus (larger sphere), NLi (smaller sphere), and centrosomes (small foci) are shown. Centrosomes are depicted in red, to indicate they contain γ-tubulin. The top row illustrates events that can be seen by DIC (gray) + γ-tubulin immunofluorescence. Centrosomes appear at approximately 4-5 minutes post-insemination. The nucleolus shrinks down into the NLi and is no longer visible by eight minutes. The NLi itself begins to dissipate at approximately 8 minutes and is no longer visible by 12. The last visible position of the NLi predicts the deeper cytoplasmic spindle pole and, with a vector drawn to the most proximal region of the cell cortex, defines the spindle axis (not shown; see references 2 and 8). The middle row depicts the fate of

nucleolar contents as observed with mcAb53. This antigen is at first distributed broadly in the nucleolus. In contrast to our expectations based on DIC images, the nucleolar contents are left behind to gradually disperse in the nucleoplasm as the nucleolus is drawn into the NLi. At approximately 8 minutes post insemination, the NLi is still visible by DIC but is completely devoid of mcAb53 staining. By 10 minutes, however, a diffuse labeling appears within the NLi and develops into a strong focal point by 12 minutes. This mcAb53-positive punctum persists for several minutes, marking the last visible position of the NLi and the future position of the internal spindle pole. The bottom row illustrates the distribution of NLi components during this process, visualized with mcAb23 for nucleolinin (NLn; purple). Present in the NLi as a slim crescent in the unactivated oocyte and through the first 2-3 minutes post-insemination, nucleolinin begins to expand over the NLi by 4 minutes. One, and then two nucleolinin-positive foci appear in the cytoplasm. These become γ-tubulin-positive centrosomes. Nucleolinin staining is sequentially lost from the centrosomes and, finally, from the NLi itself.

Clone/Contig	Size(bp)	Top Database Hit (E ≤ .01)	E-value	Algorithm
Contig 1/NLi-1 (177)	1118	Thermomonospora curvata DSM 43183, complete genome	$3e^{-3}$	tBLASTx
Contig 13 (2)	169	Canis familiaris chromosome 31, clone XX-107H22	$2e^{-10}$	BLASTn
N2C05/NLi-2	168	Homo sapiens chromosome 15 clone (+ others)	$2e^{-73}$	BLASTn
N3H05/NLi-3	248	Shewanella violacea DSS12 DNA, complete genome	$2e^{-9}$	tBLASTx
N10E02	169	Zebrafish DNA sequence from clone CH1073-417H6	$2e^{-5}$	BLASTx
N10G07	133	Oncomelania hupensis hupensis mitochondrion	$1e^{-12}$	BLASTn
N11E09	135	Spisula solidissima cnRNA86/123/186 (+ others)	$8e^{-16}$	BLASTn
N11F06	269	Spisula solidissima gene for zinc finger protein (& cnRNA190)	$7e^{-4}$	BLASTn
N15G06	95	Schistosoma mansoni genome sequence supercontig	$6e^{-5}$	BLASTn
N17A05	152	Spisula solidissima clone S1-F10_RUSS05 microsatellite	$4e^{-13}$	BLASTn
N18B02	131	Spisula solidissima gene for zinc finger protein	$3e^{-8}$	BLASTn
N19A11	415	Brachionus manjavacas MRP motif repeat 3 protein precursor	0	BLASTn
N27B08	150	Spisula solidissima gene for zinc finger protein	$2e^{-27}$	BLASTn

Table 1. Database similarities for 13 RNAs extracted from isolated NLi. The number of clones assembling into contigs 1 and 13 are indicated in parentheses in the first column. Sequences designated NLi-l, NLi-2, and NLi-3 have been confirmed by *in situ* hybridization to localize to the NLi.

Most Resembles	Accession	E-value	Species	Comments
Small nuclear RNP F (SNRNPF)	EFN72155.1	$9e^{-37}$	*Camponotus floridanus* (ant)	nuclear; RNP core protein; RNA processing
fibrillarin	XP_002730661	$8e^{-120}$	*S. kowalevskii* (acorn worm)	nuclear; RNA methylase
Histone 2A	XP_002721657	$9e^{-138}$	*Oryctolagus cuniculus* (rabbit)	nuclear; nucleosome core protein
Ribosomal protein S14	ABG81984	$8e^{-82}$	*Diaphorina citri* (psyllid - insect)	nucleolar and ribosomal (structural, 40S subunit)
Ribosomal protein L12	XP_002617234	$3e^{-89}$	*Clavispora lusitaniae* (yeast)	nucleolar and ribosomal (60S subunit)
Peroxyredoxin	XP_001946137	$7e^{-111}$	*Acyrthosiphon pisum* (aphid)	nucleolar, cytoplasmic; thiol-specific antioxidant
Tubulin β2	XP_001138713	0.0	*Pan troglodytes* (chimp)	cytoplasmic; major microtubule,spindle protein
RuvB-like 2 (reptin52, TIP49B, Rvb2)	XP_003222734	0.0	*Anolis carolinensis* (iguana)	nuclear; DNA helicase
Rab7	XP_385317	$2e^{-117}$	*Gibberella zeae* (fungus)	cytoplasmic; GTPase, vesicular trafficking
Serine/arginine-rich splicing factor 1	NP_001155687	$3e^{-134}$	*Acyrthosiphon pisum* (aphid)	nuclear; RNA splicing factor
Glc-regulated protein (BiP;GRP-78)	NP_001191581	0.0	*Aplysia californica* (sea slug)	nuclear, cytoplasmic; HSP70 - chaperone
Cyclin-dependent kinase 1	NP_001154933	$7e^{-175}$	*Nasonia vitripennis* (wasp)	nuclear, nucleolar, centrosomal; cell cycle control
Eukaryotic elongation factor 1α	CAX72187	$2e^{-129}$	*Schistosoma jap.* (parasitic worm)	nuclear (protein export); cytoplasmic (translation)
Serine/arginine-rich splicing factor 6	AAA93072	0.0	*Homo sapiens*	nuclear; RNA splicing factor
Actin 1γ	AAX29213	0.0	*Homo sapiens*	cytoplasmic, nuclear;* multifunctional, motility
DEAD box RNA helicase	XP_001658306	0.0	*Aedes aegypti* (mosquito)	nuclear; multifunctional RNA helicase
Nop56	XP_002423012	0.0	*Pediculus humanus* (lice)	nuclear; RNA processing, ribosome biogenesis
Mitochondrial ATP synthase β	XP_624156	0.0	*Apis mellifera* (honey bee)	mitochondrial; ubiquitous nt-binding, catalytic subunit
RuvB-like 1 (TIP49A, pontin, Rvb1)	XP_002734660	0.0	*S. kowalevskii* (acorn worm)	nuclear; multifunctional, DNA helicase
ATP-dependent RNA helicase DDX17	XP_003202329	0.0	*Meleagris gallopavo* (turkey)	nuclear; ATP-dependent RNA helicase
Heat shock protein gp96	NP_999808	0.0	*S. purpuratus* (sea urchin)	nuclear, cytoplasmic; DNA gyrase, histidine kinase
NOP2-like	XP_001105884	0.0	*Macaca mulatta* (rhesus)	nucleolar; RNA methyltransferase
U5 snRNP-specific protein	NP_00108028	0.0	*Xenopus laevis*	nuclear; pre-mRNA splicing factor
Elongation factor 2	XP_002122175	0.0	*Ciona intestinalis* (sea squirt)	cytoplasmic; translation elongation

Table 2. Protein components of isolated NLi. MS identifications were obtained as described in *Methods* and subsequently used in a BLASTp search to find the best-match named proteins, shown in the first column. E-values reflect the similarity between MS identifications and the BLASTp hits shown. Localization and other comments were taken from NCBI annotation sources or, when incomplete, the primary literature.

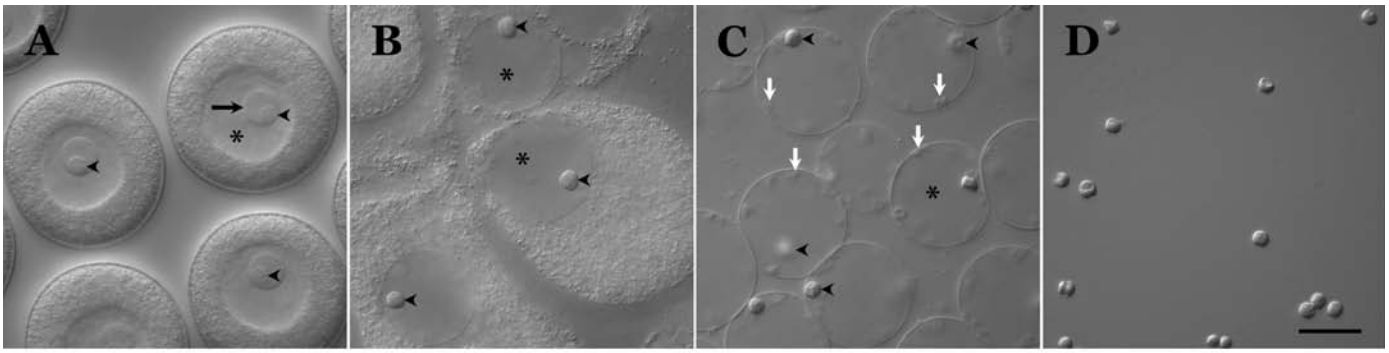

Figure 1 — Alliegro *et al.*

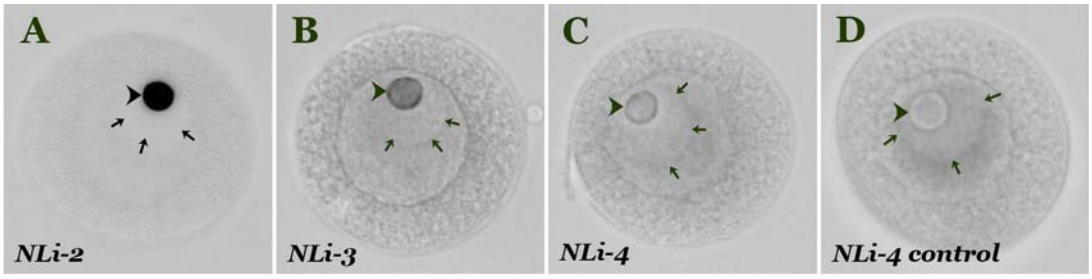

Figure 2 — Alliegro *et al.*

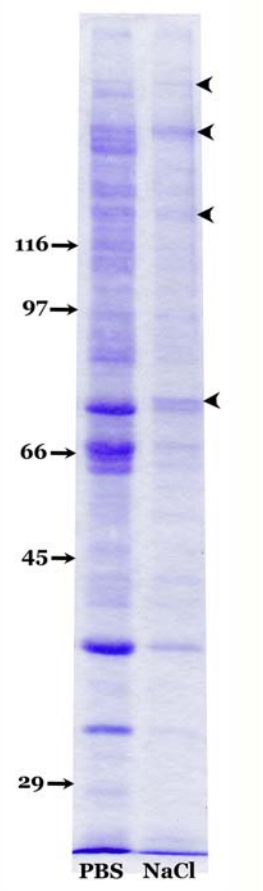

Fig. 3—*Alliegro et al.*

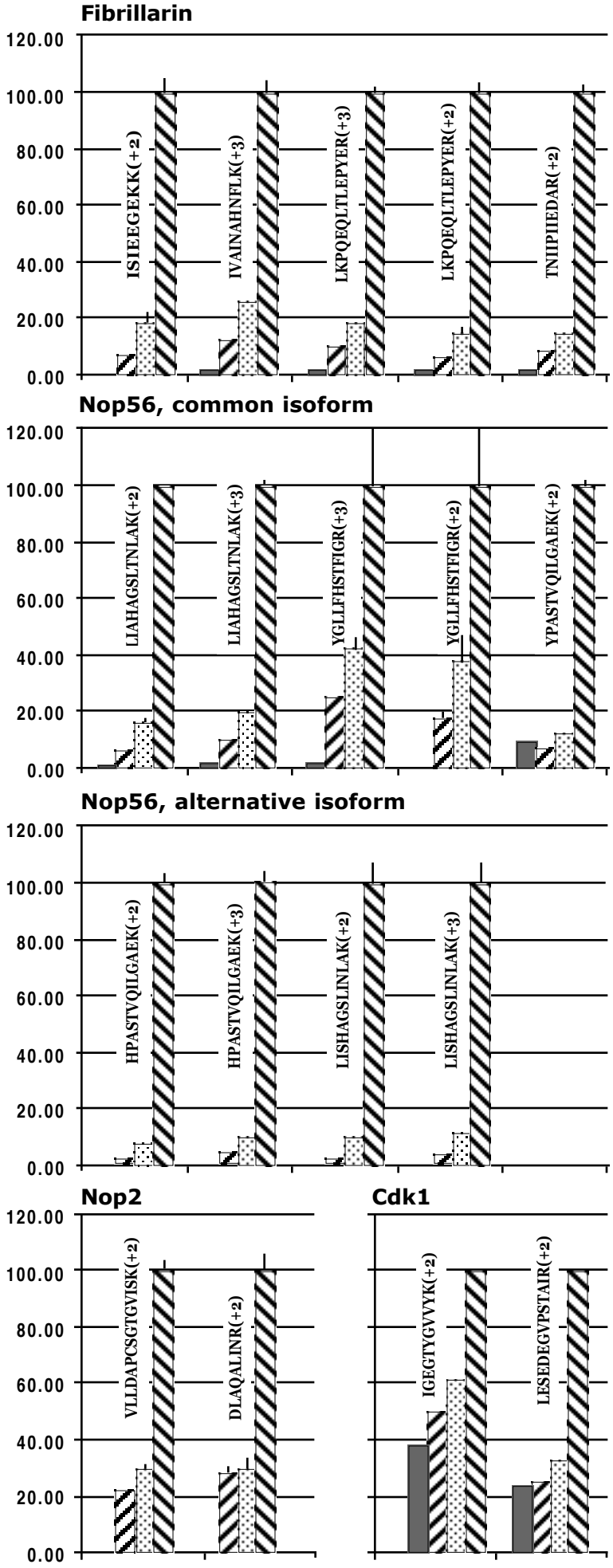

Figure 4 — *Alliegro et al.*

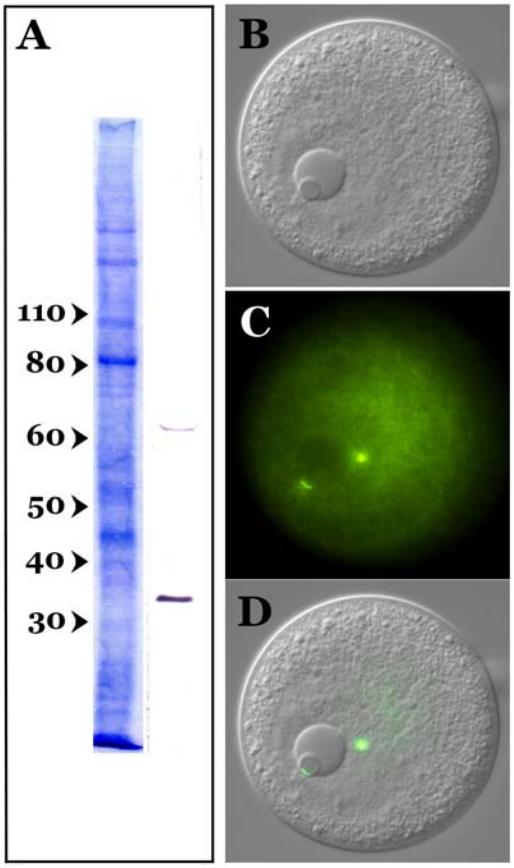

Figure 5 — Alliegro *et al.*

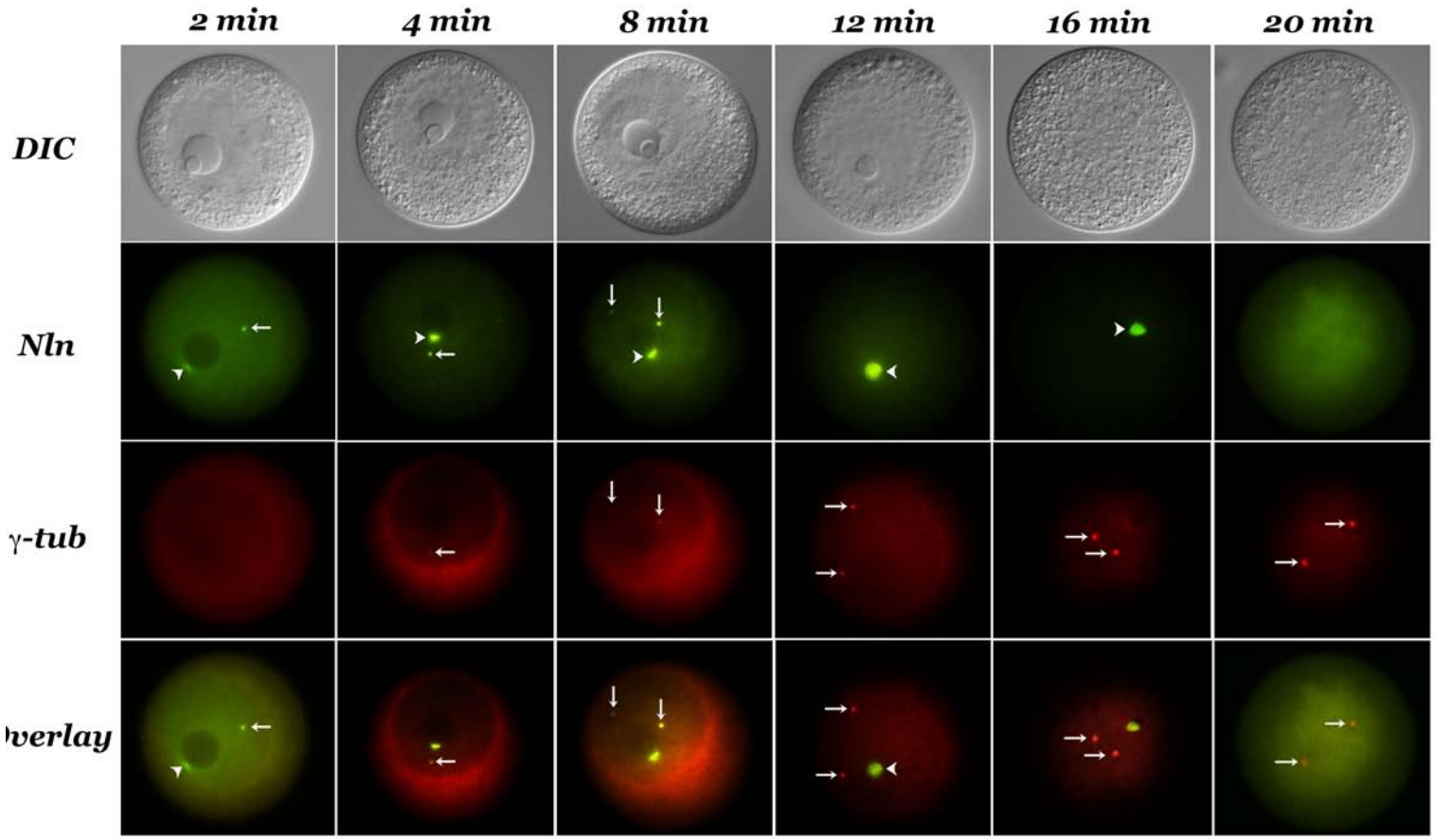

Figure 6 — Alliegro *et al.*

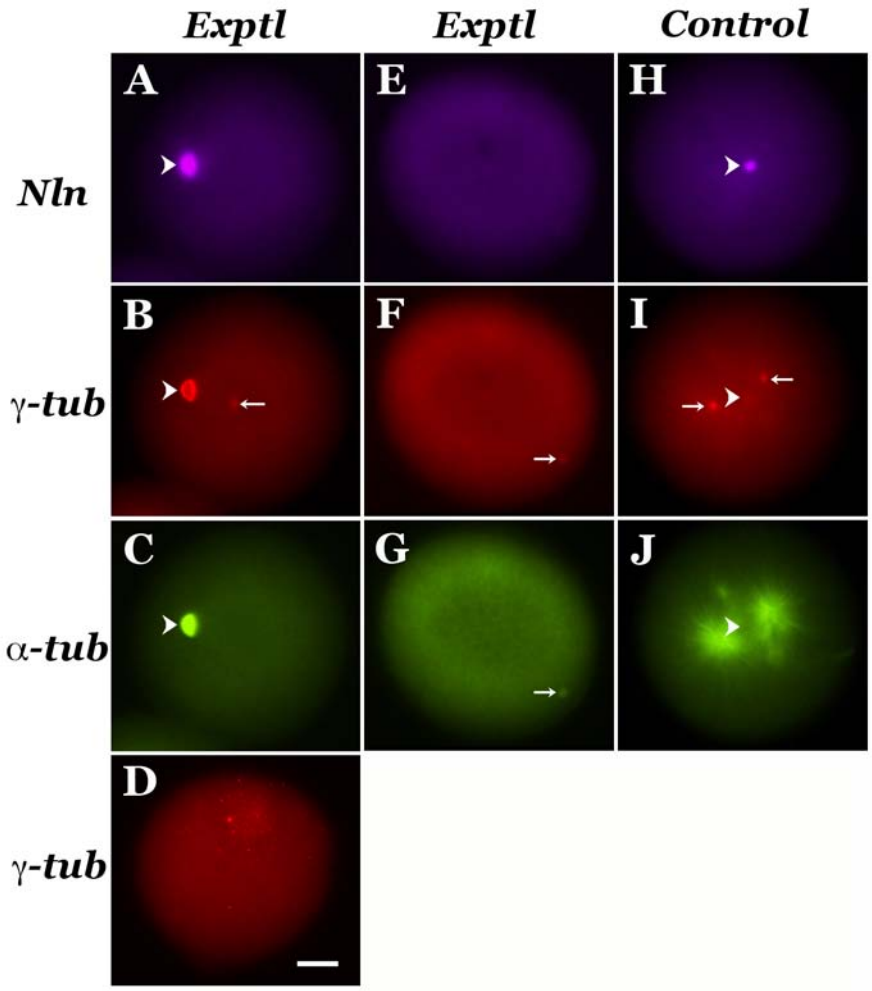

Figure 7 — Alliegro *et al.*

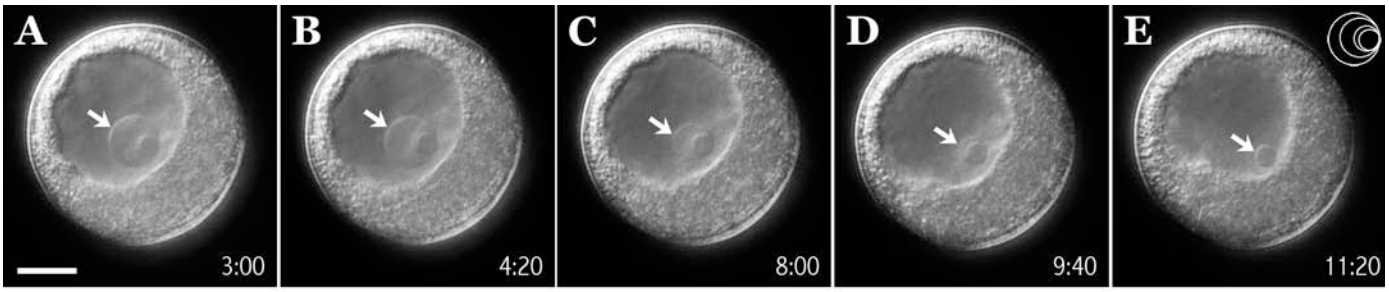

Figure 8 — Alliegro *et al.*

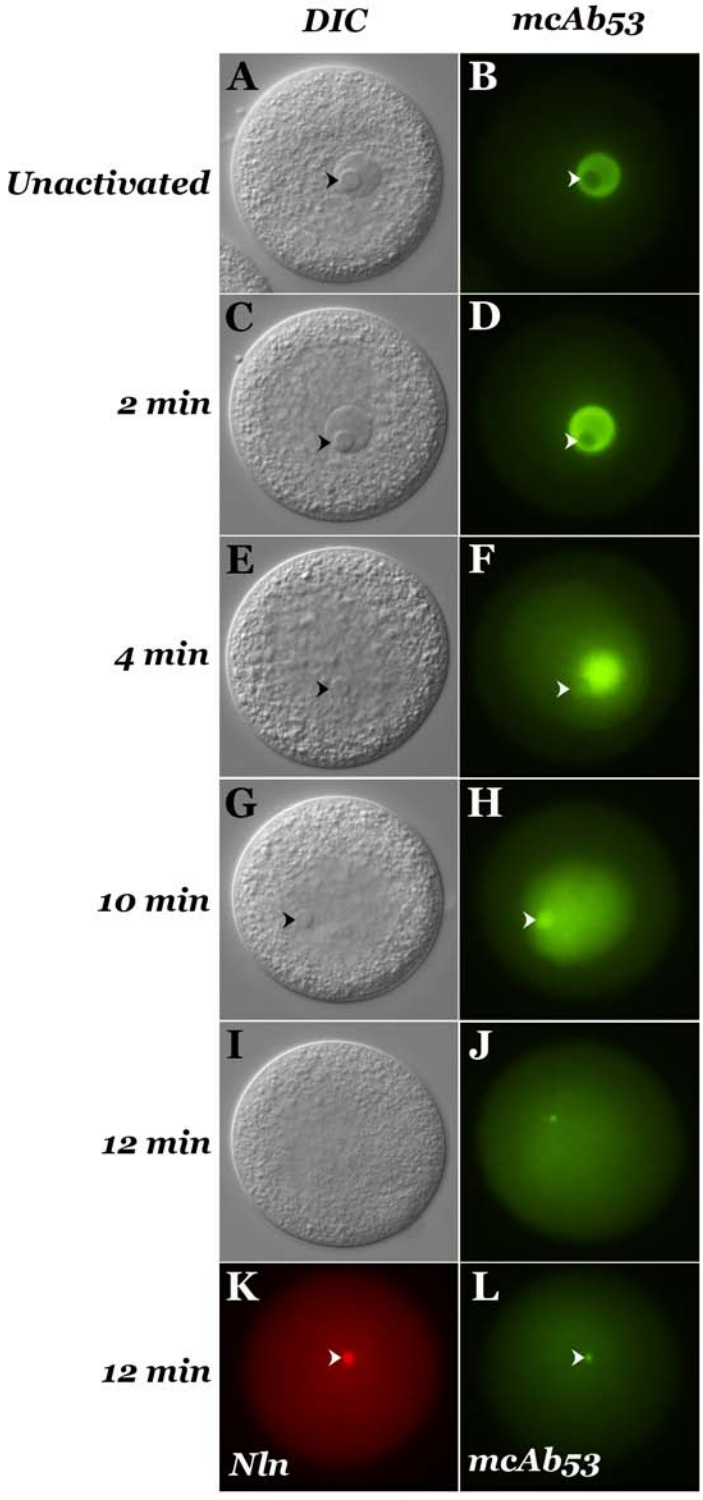

Figure 9 — Alliegro *et al.*

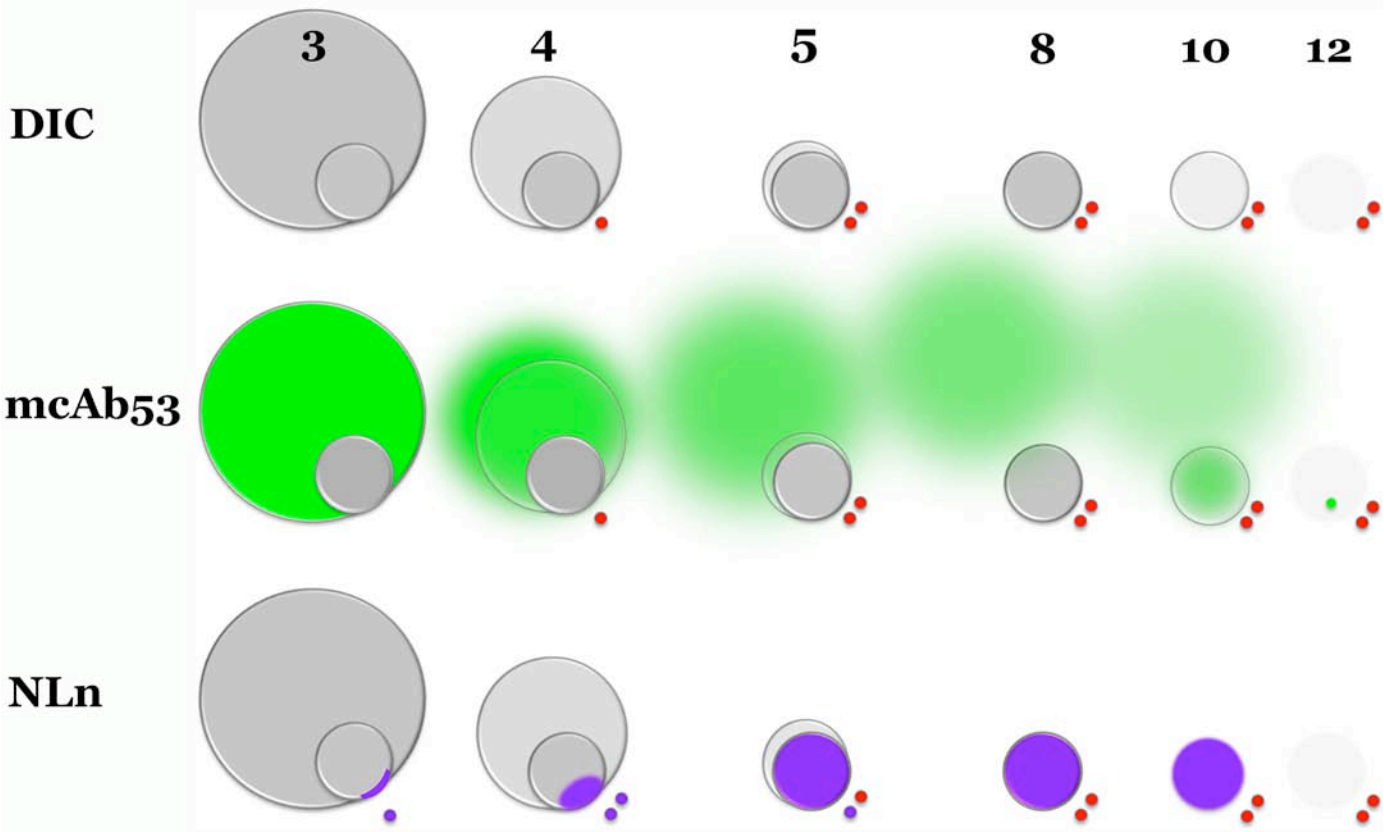

Figure 10 — Alliegro *et al.*